Measurement of cavitation induced wall shear stress

Rory Dijkink

Faculty of Science, Physics of Fluids, University of Twente,
7500 AE Enschede, The Netherlands.

Claus-Dieter Ohl

Division of Physics and Applied Physics,
School of Physical and Mathematical Sciences,
Nanyang Technological University, Singapore 637371, Singapore.

(Dated: November 4, 2008)

Abstract

The wall shear stress from cavitation bubbles collapsing close to a rigid boundary is measured with a constant temperature anemometer. The bubble is created with focused laser light and its dynamics is observed with high-speed photography. By correlating the frames, a hydrophone signal, and the wall shear stress we find that the highest stresses are created after the impact of the jet, thus during its radial spreading on the surface. The maximum of the wall shear stress varies with the power of -2.75 as a function of the distance from the jet impact and in accordance with the prediction for a steady wall impinging jet. The highest amplitude of the signal of the wall shear stresses is found for bubbles oscillating close to the boundary and reaches more than 3 kPa. Additionally, it contains a slowly decaying weaker component which may be generated by an expanding vortex ring.

Ultrasonic water bathes spotted in many labs, at opticians, and jewelers clean surfaces efficiently from attached contaminants. It is generally accepted that *not* the acoustic sound field directly but the cavitation bubbles driven by the sound field are responsible for surface cleaning [1–3]. With cleaning we refer to the process by which an attached dirt particle is at first *dislocated* and then *dragged* along with the flow. Yet, rigid boundaries on which the particle adhere limit the strength of the dragging flow: the no-slip boundary condition dictates that the lateral velocity has to ultimately drop to zero on the surface. Thus smaller dirt particles are more difficult to remove as they require a larger velocity gradient. Submicrometer sized particles are of major concern in the ultraclean processing of silicon surfaces in the chip industry [4]. Their safe to operate cleaning regime is bounded by the structural stability of nanometer sized up-patterns of modern processor and memory designs. Thus for defect free cleaning it is of utmost importance to understand the acting forces and adjust them within the structural stability limits of the patterns. In an effort to understand more on the flow we report in this letter on the time dependent velocity gradient at the surface for a single but "well controlled" cavitation bubble.

Generally, the flow strength tangent to the wall is expressed by the wall shear stress, τ_w. It is the wall normal gradient of the velocity, U, at the wall, $y = 0$, scaled by the dynamic viscosity of water, $\mu = 10^{-3}\,\mathrm{Pa\,s}$:

$$\tau_w = \mu \left. \frac{dU}{dy} \right|_{y=0}$$

To correlate this quantity with the bubble dynamics we make use of high-speed photography. In our previous work [5] we revealed that the particles on the surface are accelerated only during a very brief moment of the bubble oscillation phase; this is after a re-entrant jet has developed [6], which pierces through the lower bubble interface, and impinges onto the rigid wall [7, 8].

Ultrasound generated cavitation bubbles appear statistically and are difficult to control. Therefore, we study the flow from a single bubble generated at the focus of a pulsed laser which allows for high spatial and temporal control. A frequency doubled Nd:YAG laser (Solo PIV, New Wave, $\lambda = 532\,\mathrm{nm}$, pulse duration 6 ns) is focused at a distance h from the boundary, see Fig. 1. The origin of the cartesian xy-coordinate system is positioned on the wall with the y-axis pointing up towards the bubble center as indicated in Fig. 1. To measure the wall shear stress we make use of a resistive thin film sensor (model 55R46 from Dantec

Dynamics, Skovlunde, Denmark) located at a distance Δx from the origin. The dimensions of the active sensor area are $750\,\mu\mathrm{m} \times 200\,\mu\mathrm{m}$. The probe is connected to a anemometer (CTA, Streamline, Dantec Dynamics); and its working principle is based on the cooling of the sensor by advection [9]. It operates in a constant temperature mode, thus the signal from the CTA is proportional to the current needed to stabilize the temperature. Internally the CTA uses a feedback loop with an upper frequency of 250 kHz supplying a constant current through a Wheatstone bridge (ratio 1:20); the sensor is part of one arm of the bridge. A relation resembling King's law [9] can be derived exploiting the similarity between a temperature and a velocity boundary layer. This leads to $E^2 = A + B\tau_w^{1/n}$, where $n \approx 3$ which is in contrast to a velocity sensor with $n = 2$. From calibration measurements in channel flows we determine the constants A, B, and n for wall shear stress $0.05\,\mathrm{Pa} < \tau_w < 10\,\mathrm{Pa}$. The calibration curve is available as supplementary material.

The sensor is flush mounted in a rigid boundary which is connected to a two-axis translation stage to adjust the vertical, h, and the lateral position, Δx, with sufficient accuracy, see Fig. 1. The bubble dynamics is recorded at the same time with the wall-shear stress measurements with a high speed camera at moderate resolution (Photron APX, 128 X 96 pixels and 90.000 frames/s). Additionally, the acoustic signals from the bubble nucleation and later collapses are probed with a hydrophone (Grass 10CH, Holte, Denmark, positioned about 15mm from the laser focus). All three signals, the wall shear stress, the frame synchronization signal from the camera, and the acoustic emission are recorded simultaneously. Because of the high reproducibility of laser induced bubbles showing with the same laser power and acoustic signature we present in this Letter frames taken at higher spatial resolution and with improved illumination using a HPV-1 camera (Shimadzu Europa GmbH, Duisburg, Germany) at a resolution of 312 X 260 pixels at 250.000 frames/s. The data with lower spatial resolution but synchronous recording is available as supplementary information.

A data set from one experiment is shown in Fig. 2. It consists of three rows: on the top selected frames from the high speed recording, below the calibrated wall shear stress from the CTA, and at the bottom the acoustic signal recorded with the hydrophone. The cavitation bubble expansion and collapse cycle with a maximum bubble radius of 0.75 mm lasts for $143\,\mu$s. The first bubble expansion takes place in the first $65\,\mu$s during which the bubble flattens at the proximal side to the boundary and develops a spherical shape at the distant side. During shrinkage more liquid rushes in from the top leading to a faster shrinkage of the upper part of the bubble which is nicely visible at time 133 μs. The bubble reaches a minimum volume very close to this frame which is visible in the acoustic emission in the second row of Fig. 2 at time 143 μs. More acoustic emissions are visible, the first spike at time 0 is generated during the generation of the bubble and the third spike (at time 246 μs) during the second bubble collapse. Other lower amplitude spikes come from reflections of the pressure waves and are an acoustic signature of the container. As a side note, the acoustic propagation time from the laser focus to the hydrophone has been determined by correlating the acoustic signal with a negative spike recorded by the hot wire sensor; this is presumably caused by mild but rapid heating of the probe through the plasma emission from the focused laser pulse.

During the first bubble oscillation period - from bubble creation up to its first collapse- the recorded wall shear stress remains below 1 Pa and it is not detectable on the scale in Fig. 2. We find that the wall shear stress increases only after the acoustic emission of the collapse is recorded. A maximum in the wall shear stress of 3.5 kPa is reached 17 μs after the collapse. This amplitude is reached within 3 μs, likely limited by the bandwidth of the CTA. The shear stress signal drops quickly afterwards, reaches a second maximum and then decays exponentially on a slow timescale. Also, a third local maximum is visible right after the second bubble collapse at 246 μs. We explain the strong peak after the bubble collapse with the jet spreading radially on the surface. As the sensor is 0.25 mm away from the impact/stagnation point of the jet the delay between both reflects the travel time of the jet to the sensor. Assuming that the bubble collapse and the jet impact are occurring within a few microseconds we can estimate the velocity of the radial spreading jet to be around 15 m/s which is in the expected range [10]. The slowly decaying component of the later signal is likely caused by the expanding vortex ring [11]. However, we have no simple explanation for the second maximum and probably can only understand this when comparing with a fluid dynamics simulation. Please also note, that the sensor can only measure the absolute value of the wall shear stress, e.g. it can't detect flow reversal.

The results of many of such experiments are summarized in Fig. 3. For the further analysis the initial distance from the wall and the lateral location of the probe are now non-dimensionalized with the maximum bubble radius R_{max}, leading to the probe distance $\eta = h/R_{max}$ and stand-off parameter $\gamma = x/R_{max}$, respectively.

Outside the impact region of the jet the wall shear stress decreases with distance simply due to mass conservation. The upper group in Fig. 3 quantifies the drop of the wall shear stress by plotting the maximum of the signal as a function of η for one stand-off parameter $\gamma = 1.0 \pm 0.1$; please see the supplementary material for a discussion of the effect of spatial averaging due to a finite probe size. The wall shear stress drops within two bubble radii to about 10% from its maximum value. This supports our previous finding that bubble induced cleaning is occurring on circular patches with radii comparable to the bubble [5, 12]. Three example signals named a to c are depicted in the lower rows. Close to the impact point (a and b in Fig. 3) the amplitude of the signal changes, yet the shape remains similar. Further away (c in Fig. 3) the initial peak is strongly reduced, i.e. its magnitude is similar to the expanding vortex ring. By plotting the maximum of the wall shear stress double logarithmically we can test for a power law dependency. Glauerts similarity solution [13] of the Navier Stokes equations of a steady and infinitely thin wall jet predicts a scaling of $\tau \propto \eta^{-2.75}$. In the inset of Fig. 3 the two lines have a slope of -2.75, the solid line goes through data points for $\gamma = 1.0$ and the dashed line through a second set of data with $\gamma = 2.5$. We find good agreement between the steady similiarity solution and the measurements from an impulsive wall jetting flow. For larger distances η the signal of the wall shear probe is very weak leading to noisier measurements. Also we expect a transition of the laminar boundary to a turbulent one.

In summary we have shown, that a millimeter sized bubble collapsing close to a boundary creates intense shear stress. A wall shear stress of 3.5 kPa relates to a spatial acceleration of the flow from zero at the boundary to 3.5 m/s at only a distance of 1 μm. The bandwidth limited temporal measurements reveal that this shear stress increases from a few Pascals to 3.5kPa within 3 μs or less. This remarkable fluid dynamics has its origin in the symmetry breaking of the spherical flow by the boundary leading to the focused and high-speed jet.

The authors are thankful for the financial support through VIDI (The Netherlands Organisation for Scientific Research, NWO) and Singapore's Ministry of Education through grant number T208A1238.

---

[1] V.S. Moholkar, M.C.G. Warmoeskerken, C.D. Ohl, A. Prosperetti, AIChE J. **50**, 58 (2004).

[2] D. Krefting, R. Mettin, W. Lauterborn, Ultrasonics Sonochem. **11**, 119 (2004).

[3] F. Holsteyns, Removal of nanoparticulate contaminants from semiconductor substrates by megasonic cleaning, PhD thesis 2008, K. U. Leuven, Belgium.

[4] K. Xu, R. Vos, G. Vereecke, G. Doumen, W. Fyen, P.W. Mertens, M.M. Heyns, C. Vinckier, J. Fransaer, F. Kovacs, J. Vac. Sci. Technol. B **23**, 2160 (2005).

[5] C.D. Ohl, M. Arora, R. Dijkink, V. janve, and D. Lohse, Appl. Phys. Lett **89**, 74102 (2006).

[6] B.W. Zeff, B. Kleber, J. Fineberg, and D.P. Lathrop, Nature **403**, 401 (2000).

[7] M.S. Plesset and R.B. Chapman, J. Fluid Mech. **47**, 283 (1971).

[8] E.A. Brujan, G.S. Keen, A. Vogel, and J.R. Blake, Phys. Fluids **14**, 85 (2002).

[9] H.H. Bruun, Hot-wire Anemometry Principles and Signal Analysis, Oxford University Press 1995.

[10] Private communication Evert Klaseboer April 2008.

[11] T.B. Benjamin, and A.T. Ellis, Phil. Trans. R. Soc. Lond. A **260**, 221 (1966).

[12] C.D. Ohl, M. Arora, R. Ikink, N. de Jong, M. Versluis, M. Delius, and D. Lohse, Biophys. J. **91**, 4285 (2006).

[13] M.B. Glauert, J. Fluid Mech. **1**, 625 (1956).

Figure captions

Fig. 1: Sketch of the geometry of the experiment to correlate the wall shear stress with the bubble dynamics. The bubble is generated at the laser focus at xy-position $(0, h)$. The center of the probe is located at $(\Delta X, 0)$.

Fig. 2: Simultaneous measurement of the bubble shape, the acoustic emission, and the shear stress exerted on the boundary. The selected frames in the top row present the bubble pulsation close to a boundary. The bottom part of each frame is a reflection from the boundary and helps to locate the position of the wall. The bubble collapses aspherically with the formation of a reentrant jet and deforms during re-expansion into a pancake shape. Acoustic emission (third row) is recorded during the bubble creation and bubble collapses; yet, intense shearing of the liquid close to the boundary (second row, measured at the marked position in the first frame) is only observed $17\,\mu$s after the first collapse. Thus maximum wall shear stress is not occurring during bubble collapse but when the radial spreading jet flows across the sensor. The maximum bubble radius is 0.75mm and the bubble is created 0.8mm away from the boundary. The dashed vertical lines indicate the time of the picture taken and depicted in the top row.

Fig. 3: In the upper part of the figure the maximum of the wall shear stress as a function of the distance η for a stand-off distance of $\gamma = 1.0$ is plotted. At the three marked positions a, b and c the time resolved signals are displayed below. The inset of the upper plot depicts the wall shear stress double logarithmically and is compared to the Glauert solution [13] with a similarity exponent of -2.75 ($\bullet$ for $\gamma = 1.0 \pm 0.1$ and $\diamondsuit$ for $\gamma = 2.5 \pm 0.2$).

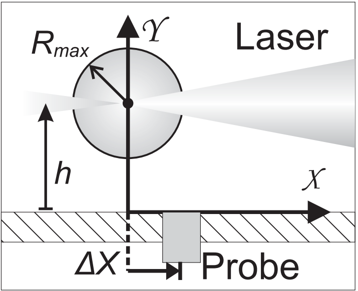
Υ
Laser
R_{max}
h
X
ΔX
Probe

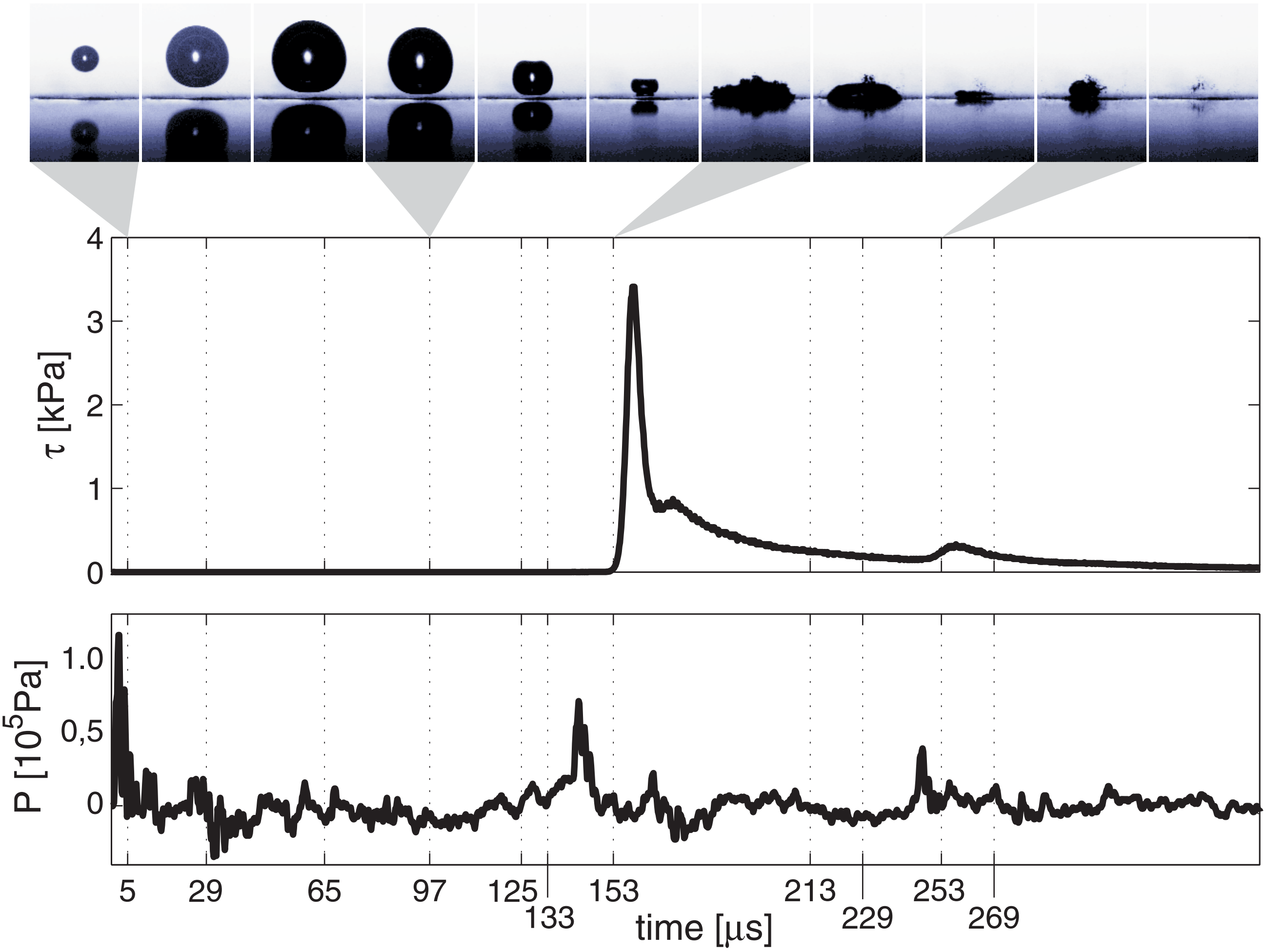
τ [kPa]
4
3
2
1
0
P [10^5Pa]
1.0
0,5
0
5
29
65
97
125
133
153
213
229
253
269
time [µs]

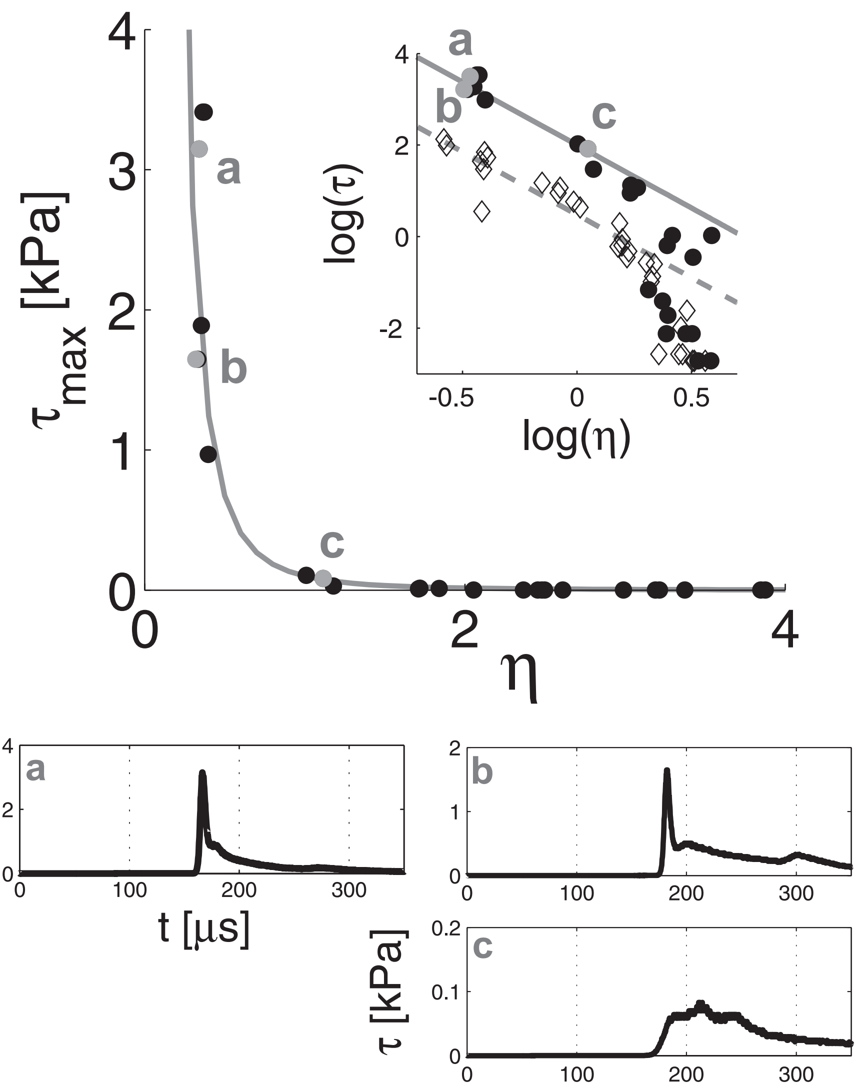
τ_{max} [kPa]
0
1
2
3
4
η
0
2
4
a
b
c
log(τ)
log(η)
4
2
0
-2
-0.5
0
0.5
a
b
c
t [μs]
τ [kPa]
0
2
4
0
100
200
300
a
0
1
2
0
100
200
300
b
0
0.1
0.2
0
100
200
300
c